INTERNATIONAL JOURNAL FOR NUMERICAL METHODS IN FLUIDS, VOL. 21, 401–411 (1995)

NUMERICAL SIMULATION OF AXISYMMETRIC UNSTEADY INCOMPRESSIBLE FLOW BY A VORTICITY–VELOCITY METHOD

YUAN LI, FU DEXUN AND MA YANWEN

LNM, Institute of Mechanics, Chinese Academy of Sciences, Beijing 100080, People's Republic of China

SUMMARY

A new numerical method for solving the axisymmetric unsteady incompressible Navier–Stokes equations using vorticity–velocity variables and a staggered grid is presented. The solution is advanced in time with an explicit two-stage Runge–Kutta method. At each stage a vector Poisson equation for velocity is solved. Some important aspects of staggering of the variable location, divergence-free correction to the velocity field by means of a suitably chosen scalar potential and numerical treatment of the vorticity boundary condition are examined. The axisymmetric spherical Couette flow between two concentric differentially rotating spheres is computed as an initial value problem. Comparison of the computational results using a staggered grid with those using a non-staggered grid shows that the staggered grid is superior to the non-staggered grid. The computed scenario of the transition from zero-vortex to two-vortex flow at moderate Reynolds number agrees with that simulated using a pseudospectral method, thus validating the temporal accuracy of our method.

KEY WORDS: unsteady incompressible flow; vorticity–velocity formulation; numerical simulation; staggered grid; spherical Couette flow

1. INTRODUCTION

In the numerical simulation of incompressible flows the appropriate mathematical formulation of the Navier–Stokes (N–S) equations may be advantageous if the choice is according to the problem domain and boundary conditions. Two distinctly different formulations have been utilized in the literature. In the first formulation the momentum equation, which contains both velocity and pressure, is solved numerically with a derived Poisson equation for pressure (i.e. pressure–velocity or primitive variable formulation[1]). The second formulation is based on eliminating the pressure from the momentum equation by application of the curl operator; in this manner a vorticity transport equation is solved in lieu of the momentum equation (vorticity–velocity formulation[2,3]). As demonstrated in Reference 4, the vorticity–velocity ($\boldsymbol{\omega}$–$\mathbf{u}$) formulation has a striking advantage over the other when applied to problems in a non-inertial frame of reference, because the non-inertial effects only enter into the solution of the problem through the implementation of initial and boundary conditions. Another advantage of the $\boldsymbol{\omega}$–$\mathbf{u}$ formulation may be the easier implementation of the vorticity boundary condition than that of the pressure boundary condition. Moreover, the vorticity is calculated directly and is convenient in characterizing certain features of the flow.

The idea of using an $\boldsymbol{\omega}$–$\mathbf{u}$ formulation itself is not new. In Reference 2 the $\boldsymbol{\omega}$–$\mathbf{u}$ form was used for calculating steady incompressible flows in three dimensions. The formulation was also applied to solve unsteady two-dimensional flows[5,6] and three-dimensional flow.[7] Generally the vorticity was obtained from the vorticity transport equation and the velocity from the Poisson equation or directly from Cauchy–Riemann equations composed of the continuity equation and vorticity definition.[7]

CCC 0271–2091/95/050401–11

Received July 1994
Revised January 1995

In the present paper a numerical method in terms of the vorticity–velocity for solving the axisymmetric unsteady incompressible N–S equations is developed. The three vorticity transport equations and three Poisson equations for velocity components are retained as in general 3D flows. The solenoidality constraints of the velocity and vorticity fields require a coupled solution between the vorticity transport equations and the velocity Poisson equations. Unfortunately, the number of unknowns and the presence of the non-linear advective-stretching terms prohibit the use of a direct solver; thus iterative methods were often needed.[2,3,7] The solution for an unsteady flow might be very time-consuming, since many iterations are needed at each physical time step. Furthermore, even with the coupling between the dynamic and kinematic features the solenoidality constraints of the velocity and vorticity fields are not necessarily satisfied, owing to other sources such as errors in the discretization or improper treatment of the vorticity boundary condition.

There are two types of approach to deal with the solenoidality problem in the past literature. In the first approach the solenoidal components were obtained by solving a Poisson equation for a suitably chosen scalar potential.[7,8] In the second approach a staggered grid was adopted.[9] The present method incorporates the merits of References 7–9 in two ways: first, the variables are located on a staggered grid and a conservative form of the vorticity transport equations is adopted in order to satisfy the solenoidality constraint of the velocity and vorticity fields on individual cells; second, the velocity field is projected onto a solenoidal component by using Helmholtz decomposition in order to reduce the deviation from the solenoidal field. However, the present method differs from previous ones mainly in two features: (i) the numerical scheme to integrate the vorticity transport equations in time is an explicit two-stage Runge–Kutta method and the Poisson equations for velocity components are solved by an SOR method instead of an ADI method (which might involve solving a block matrix equation in non-Cartesian co-ordinates); (ii) the velocity field is projected onto a solenoidal component by using a suitably chosen scalar potential at each stage in each physical time step.

An explicit time integration method appears to be more efficient than implicit methods. The reasons why we use a two-stage instead of a higher-stage Runge–Kutta algorithm are that its accuracy is consistent with second-order spatial accuracy and that our case is a moderate-Reynolds-number and low-wave-number flow. The correction to the velocity field by Helmholtz decomposition helps in satisfying better the divergence-free constraint at each physical time level. Although the proposed method does not include iteration between the vorticity transport equations and the Poisson equations, it is still at least first-order temporally accurate and the computed results agree with those of high-resolution simulation using a second-order temporally accurate pseudospectral method.[10]

In Section 2 the differential formulation of the problem and a solution procedure are presented. Section 3 describes the discretization of the equations and vorticity boundary condition. In Section 4 the method is applied to a test problem of spherical Couette flow at $Re = 800$ with a gap ratio $\sigma = 0{\cdot}18$. Comparison with other numerical[10] and experimental results[11] is also presented.

2. VORTICITY–VELOCITY FORMULATION OF N–S EQUATIONS AND SOLUTION PROCEDURE

2.1. *Mathematical formulation*

The non-dimensional vorticity–velocity form of the Navier–Stokes equations for laminar flow of an incompressible Newtonian fluid can be written in the conservative form[9]

$$\frac{\partial \boldsymbol{\omega}}{\partial t} = \nabla \times (\mathbf{u} \times \boldsymbol{\omega}) + \frac{1}{Re} \nabla^2 \boldsymbol{\omega}, \tag{1}$$

$$\nabla^2 \mathbf{u} = -\nabla \times \boldsymbol{\omega}. \tag{2}$$

Here $\mathbf{u} = \mathbf{u}(\mathbf{x}, t)$ and $\boldsymbol{\omega} = \boldsymbol{\omega}(\mathbf{x}, t)$ are the velocity and vorticity fields respectively, $\mathbf{x}$ is a point, t is time and $Re = U_{\text{ref}} L_{\text{ref}}/\nu$, where U_{ref} is the reference velocity, L_{ref} is the reference length and ν is the kinematic viscosity.

The vorticity transport equation (1) is derived by applying the curl operator to the momentum equations, whose advective term is written in Lagrange form. The velocity Poisson equation (2) results from taking the curl operator of the vorticity definition and using the continuity equation. We denote ∇^2 as a Laplacian operator in Cartesian co-ordinates but not in cylindrical or spherical co-ordinates.

Equations (1) and (2) must be solved in some domain Ω with a boundary B subject to the initial conditions

$$\mathbf{u} = \mathbf{u}_0 \quad \text{and} \quad \boldsymbol{\omega} = \boldsymbol{\omega}_0 \quad \text{at} \quad t = 0 \tag{3a, b}$$

and the boundary conditions

$$\mathbf{u} = \mathbf{u}_B \quad \text{and} \quad \boldsymbol{\omega} = (\nabla \times \mathbf{u})|_B \tag{4a, b}$$

on the boundary B of Ω.

2.2. *Solution procedure*

The task is to develop a second-order spatially and at least first-order temporally accurate numerical algorithm for the system described in equations (1)–(4). To seek the solution at $t = T$, we divide the time from t_0 to T into subintervals. Within any fixed time interval a two-stage explicit Runge–Kutta method is constructed to advance the solution from the start to the end of that time interval. Let the superscript l indicate the value at the end of the first stage. The solution procedure may be summarized in the following steps.

(i) Integrate the vorticity transport equation (1) in time to constitute the first stage of the Runge–Kutta method,

$$\mathbf{K}_1 = \Delta t \left(\nabla \times (\mathbf{u}^n \times \boldsymbol{\omega}^n) + \frac{1}{Re} \nabla^2 \boldsymbol{\omega}^n \right), \tag{5a}$$

so that the vorticity $\boldsymbol{\omega}^l$ in the interior of the domain Ω is obtained from

$$\boldsymbol{\omega}^l = \boldsymbol{\omega}^n + \mathbf{K}_1. \tag{5b}$$

(ii) Solve the Poisson equation

$$\nabla^2 \hat{\mathbf{u}}^l = -\nabla \times \boldsymbol{\omega}^l \tag{6}$$

under the boundary condition (4a).

The intermediate solution $\hat{\mathbf{u}}^l$ may not be solenoidal, since $\boldsymbol{\omega}^l$ is determined using $\mathbf{u}^n$. However, the Helmholtz theorem allows us to project $\hat{\mathbf{u}}^l$ onto a solenoidal component and an irrotational component. Details of the projection procedure will be given in Section 3.2. We call this solenoidal component $\mathbf{u}^l$.

(iii) Use equation (4b) to obtain the vorticity boundary condition for the second stage,

$$\boldsymbol{\omega}_B^l = (\nabla \times \mathbf{u}^l). \tag{7}$$

The normal component of $\boldsymbol{\omega}_B^l$ is known exactly if the velocity boundary condition is given as equation (4a), but the tangential component is not known *a priori*. For the computation of viscous terms in the second stage the vorticity on the boundary is taken directly as $\boldsymbol{\omega}_B^l$. This might result in $O(\Delta t)$ error on the boundary.

(iv) Construct the second stage of the Runge–Kutta method,

$$\mathbf{K}_2 = \Delta t\left(\nabla \times (\mathbf{u}^l \times \boldsymbol{\omega}^l) + \frac{1}{Re}\nabla^2 \boldsymbol{\omega}^l\right), \tag{8a}$$

to obtain the vorticity at the end of time step n or at the beginning of time step $n+1$ as

$$\boldsymbol{\omega}^{\nu++} = \boldsymbol{\omega}^{\nu} + ''\cdot = (\mathbf{K}_+ + \mathbf{K}_-). \tag{8b}$$

(v) Again solve the Poisson equation

$$\nabla^2 \hat{\mathbf{u}}^{n+1} = -\nabla \times \boldsymbol{\omega}^{n+1} \tag{9}$$

under the boundary condition (4a) and then project the computed velocity field onto a solenoidal component $\mathbf{u}^{n+1}$. We take this solenoidal component $\mathbf{u}^{n+1}$ as the velocity solution at the new time level.

(vi) Use the vorticity definition (4b) to obtain the vorticity on the boundary B for the new time level. Go back to (i) to begin the computation for the next time step.

The solution pair ($\boldsymbol{\omega}$, $\mathbf{u}$) satisfies the vorticity–velocity formulation of the N–S equations (1)–(4), but with a little time lagging in the vorticity boundary condition. Actually, only the tangential component of $\boldsymbol{\omega}_B$ is determined in terms of $\mathbf{u}_B$ and $\mathbf{u}$ in the interior, which requires an approximation to the normal derivative of the velocity on the boundary B. Since the tangential component of $\boldsymbol{\omega}_B$ is proportional to the shear stress, care must be taken in discretizing the vorticity boundary condition (4b). In addition, the solenoidality of the velocity and vorticity fields requires appropriate location of the variables on the grid, which will be discussed in the next section.

3. DISCRETIZED SCHEME

3.1. *Spatial discretization*

Since the problem to be solved involves flow in a spherical gap, spherical co-ordinates are suitable for the computation. Let r be the radial co-ordinate and θ be the circumferential angle. Because of axisymmetry, we consider only the half-sphere shown in Figure 1. The domain Ω is partitioned into quadrilateral cells according to co-ordinate lines. The location of the staggered variables is shown in Figure 2, which is a 2D projection of the 3D version.[9] Non-staggered variable location is also used for comparison with the staggered case.

The first- and second-order spatial derivatives are replaced with second-order central differences. The location of variables on grids is an important factor, at least in determining how well the continuity equation is satisfied in a discrete sense. In the present $\boldsymbol{\omega}$–$\mathbf{u}$ formulation, mass conservation requires the total flux to be zero across the cell sides. When the velocity components are located at the cell mid-sides, mass conservation can be satisfied to round-off error level. The conservative form of the vorticity transport equation will play an essential role in the satisfaction of mean vorticity conservation.[9] This form also helps in satisfying the solenoidality of the vorticity field if the vorticity components are staggered as shown in Figure 2. Furthermore, the staggered variable location guarantees the two-point formula an accuracy of $(\Delta x/2)^2$ in the discretization of the first derivative instead of $(\Delta x)^2$ that can be obtained using a non-staggered variable location. This is particularly clear in the computation of the right-hand side of equation (2).

The vorticity is obtained explicitly from the discretized forms of equations (5a), (5b), (8a) and (8b). The discretized Poisson equation (6) or (9) at P_{u_i} connects five u_i variables at four neighbouring u_i locations. On boundaries where u_{i-1} or u_{i+1} is exterior to the domain Ω it is extrapolated from the values on the boundary and at the first interior location, e.g. $u_{i-1} = 2u_B - u_i$. This treatment results in

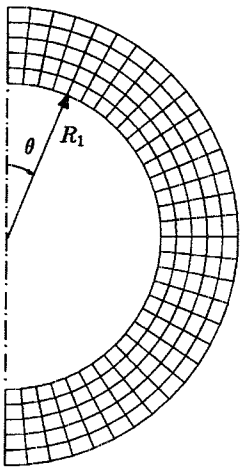

Figure 1. Spherical co-ordinates and grid of solution domain

faster convergence in iterating the Poisson equation, as the numerical test indicated. The discretized Poisson equation can be cast in the form

$$a_W u_{i-1,j} + a_E u_{i+1,j} + a_S u_{i,j-1} + a_N u_{i,j+1} + a_P u_{i,j} = r_{i,j}, \tag{10}$$

where a_W, a_E, a_S, a_N and a_P are constant coefficients related to co-ordinates and mesh sizes and $r_{i,j} = r(u_{i,j}, v_{i,j}, w_{i,j}, \boldsymbol{\omega})$ is the residual of the discretized form of equation (6) or (9). The three linear equations are coupled, because the $r_{i,j}$ depend on other components to be solved. A scalar type of point SOR iteration method is applied for each of the three equations; vectorization of the code is obtainable on the $i+j=\text{const.}$ plane.

3.2. *Divergence-free correction to the velocity field*

The velocity obtained from equation (6) or (9) may not be solenoidal, though adoption of the staggered grid may improve the results. This is particularly true when the transition is fast. We now decompose the velocity $\hat{\mathbf{u}}$ into a solenoidal part $\mathbf{u}$ and an irrotational part $-\nabla\phi$,

$$\hat{\mathbf{u}} = \mathbf{u} - \nabla\phi, \tag{11}$$

in domain Ω.

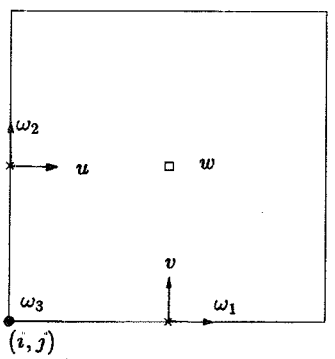

Figure 2. Grid cell showing staggered location of flow variables. The reference point (i, j) is marked with a solid circle

A Poisson equation for the scalar ϕ is obtained by taking the divergence of equation (11),

$$\nabla^2\phi = -\nabla\cdot\hat{\mathbf{u}} \quad \text{in} \quad \Omega, \tag{12}$$

which is to be solved with the Neumann boundary condition

$$\mathbf{n}\cdot\mathbf{u} - \mathbf{n}\cdot\hat{\mathbf{u}} = 0$$

or

$$\frac{\partial\phi}{\partial n} = 0 \quad \text{on} \quad B. \tag{12b}$$

This condition comes from the fact that the normal component of $\hat{\mathbf{u}}$ on the boundary exactly equals the specified value if the velocity boundary condition is given as equation (4a). To maintain second-order accuracy, the variable ϕ is located at the centre of each cell. The discretized Poisson equation is solved using a direct matrix solver, but it can also be solved by other methods such as line SOR. Once ϕ has been obtained, the solenoidal velocity is obtained as

$$u = \hat{u} + \frac{\partial\phi}{\partial r}, \tag{13a}$$

$$v = \hat{v} + \frac{\partial\phi}{r\partial\theta}. \tag{13b}$$

3.3. *Treatment of vorticity boundary condition*

In describing the formulation of the N–S equations in Section 2.1, we assumed that the velocity was specified on the boundary, then the vorticity was computed by definition (4b). According to the vorticity definition, the normal derivatives of velocity need to be approximated. Usually N-point one-sided differencing is used to evaluate $\partial u_i/\partial n$ on B. Generally speaking, the velocity might not be specified on all boundary segments. However, equation (4b) does represent the condition on each boundary segment. Because the most difficult yet most important portion is on the body surface, proper treatment should be applied in approximating $\partial u_i/\partial n$ on the wall. Other boundary segments seem not so critical as the solid body surface.

There is a contradiction in approximating $\partial u_i/\partial n$ on the non-staggered grid. On one hand, $\partial u_i/\partial n$ can be evaluated by three-point one-sided differencing in order to obtain a second-order-accurate vorticity boundary condition, but this often results in numerical instability as shown by Roache.[12] In our spherical Couette flow problem $\partial w/\partial n$ is responsible for the numerical instability, since the azimuthal flow (w-component) is dominant. On the other hand, a two-point formula can be numerically stable, but it causes the boundary condition for the vorticity to be less accurate. A remedy might be to solve equations (1) and (2) iteratively together with a second-order-accurate three-point formula for the vorticity boundary condition, but a large number of iterations might be needed, making the method impractical for simulating unsteady flow.

On the staggered grid the vorticity components are

$$\omega_1 = \frac{1}{r\theta}\frac{\partial(\sin\theta w)}{\partial\theta}\bigg|_B, \tag{14a}$$

$$\omega_2 = -\left(\frac{\partial w}{\partial r} + \frac{w}{r}\right)\bigg|_B, \tag{14b}$$

$$\omega_3 = \frac{1}{r}\left(\frac{\partial(rv)}{\partial r} - \frac{\partial u}{\partial\theta}\right)\bigg|_B. \tag{14c}$$

The normal derivative $\partial/\partial r$ is replaced by the two-point one-sided difference between the wall and the first velocity location at distance $\frac{1}{2}\Delta r$ from the wall. In spite of being first-order-accurate, the two-point formula on the staggered grid has half the truncation error of that on the non-staggered grid. Moreover, the better satisfaction of the solenoidality constraint of the velocity and vorticity fields on the staggered grid may help to improve the accuracy in evaluating the vorticity boundary condition on the body surface.

4. RESULTS OF TEST PROBLEM

The flow between two concentric rotating spheres in which the outer sphere is held stationary and the inner one is rotated at an angular velocity Ω_1 has been widely studied.[10,11] This flow is well known for its multiple steady, stable solutions at Reynolds numbers greater than a critical value. We chose this flow as a test case because the balance of torques acting on the inner and outer spheres in a stable steady state provides an important criterion for validation and comparison purposes. The transition from zero-vortex to two-vortex flow at $Re_1 = \Omega_1 R_1^2/\nu = 800$ for a gap ratio $\sigma = 0{\cdot}18$ is unique if the Reynolds number suddenly increases from zero to 800.

The computation is started from the Stokes flow

$$u = 0, \qquad v = 0, \qquad w = \frac{R_1^3 R_2^3}{R_2^3 - R_1^3}\left[\left(\frac{1}{r^3} - \frac{1}{R_2^3}\right)\Omega_1 + \left(\frac{1}{R_1^3} - \frac{1}{r^3}\right)\Omega_2\right] r \sin\theta. \tag{15}$$

4.1. *Comparison of results between staggered and non-staggered grids*

The influence of the variable location on the grid has been studied first to determine which grid is better. A typical 21 (r) × 129 (θ) grid is selected. Using the time step $\Delta t = 0{\cdot}025$, both computations reach an asymptotic steady state after about 5000 time steps. The vorticity distributions on the inner ($r = (R_1 + R_2)/2$) and outer spheres are compared in Figures 3(a)–3(c). The difference is obvious on the spheres but trivial in the interior region. The torque coefficients and norms of divergence of velocity and vorticity are listed in Table I. The torque coefficient is defined as

$$\tau = \frac{M}{\frac{1}{2}\rho R_1^5 \Omega_1^2} = \frac{4\pi}{Re}\int_0^\pi \sin^2\theta\left(-\omega_2) - \frac{w}{r}\right)\Big|_w \, \mathrm{d}\theta. \tag{16}$$

Surprisingly, the torques acting on the inner and outer spheres as computed using the non-staggered grid are in significant imbalance; however, this discrepancy may be understood by considering the difference between Figures 3(a) and 3(c) and the poor satisfaction of the solenoidality constraint of the velocity and vorticity fields on the non-staggered grid seen in Table I. In contrast, the staggered grid ensures good torque balance at steady state. This comparison suggests that the staggered grid is preferable. In the following computations only the staggered grid is used.

4.2. *Mesh sensitivity*

To validate the present **ω–u** method with the staggered variable location, a mesh dependence study has been conducted. Three grids are adopted. The results of the mesh sensitivity analysis are presented in Table II in terms of torque coefficient, first-vortex size near the equator, maximum axial velocity and maximum circumferential vorticity on the inner sphere at steady state.

We see that the torque is greater than 0·216 and the first-vortex size is above 0·9, which are the experimental results,[11] but as the grid is refined, the values improve.

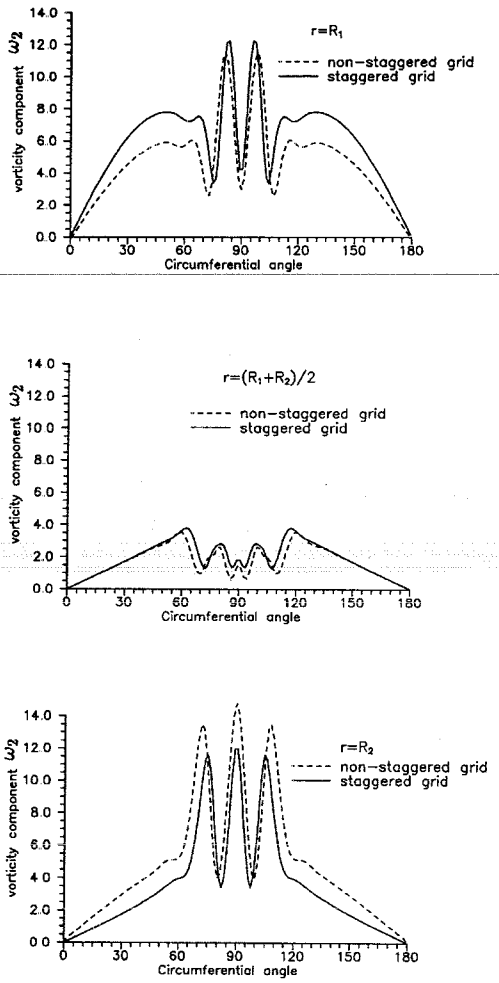

Figure 3. Comparison of steady state distributions of vorticity component ω_2 along circumferential direction, grid 21 × 129, $\Delta t = 0.025$; $\theta = 90°$ corresponds to the equator

Table I. Torques and average norms of divergence of velocity and vorticity

Variable location	τ_1	τ_2	$\| \nabla \cdot \hat{\mathbf{u}} \|$	$\| \nabla \cdot \mathbf{u} \|$	$\| \nabla \cdot \boldsymbol{\omega} \|$
Non-staggered	0.189	0.285	8.8×10^{-3}	1.34×10^{-3}	2.09
Staggered	0.2209	0.2211	8.0×10^{-6}	1.56×10^{-7}	1.44×10^{-2}

Note: $\| \nabla \cdot \hat{\mathbf{u}} \|$ is the value before projection.

Table II. Mesh dependence results

Grid	τ	First-vortex size	$u_{\max}\|_{\theta=\pi/2}$	$\omega_{2\max}\|_{r=R_1}$
21×65	0.223	0.912	0.073	13.12
21×129	0.221	0.918	0.086	12.25
31×129	0.220	0.906	0.084	12.82

4.3. Zero-vortex–two-vortex (0 → 2) transition and comparison with other numerical results

One important question is how temporally accurate the present method actually is. In Reference 10 a high-resolution simulation of the 0 → 2 transition has been conducted using a pseudospectral method. The initial state is that of Stokes flow and *Re* increases suddenly from zero to 800. The authors used the time step $\Delta t = 2\pi/70$. We use $\Delta t = 0{\cdot}025$ in our computation owing to the limitation of numerical

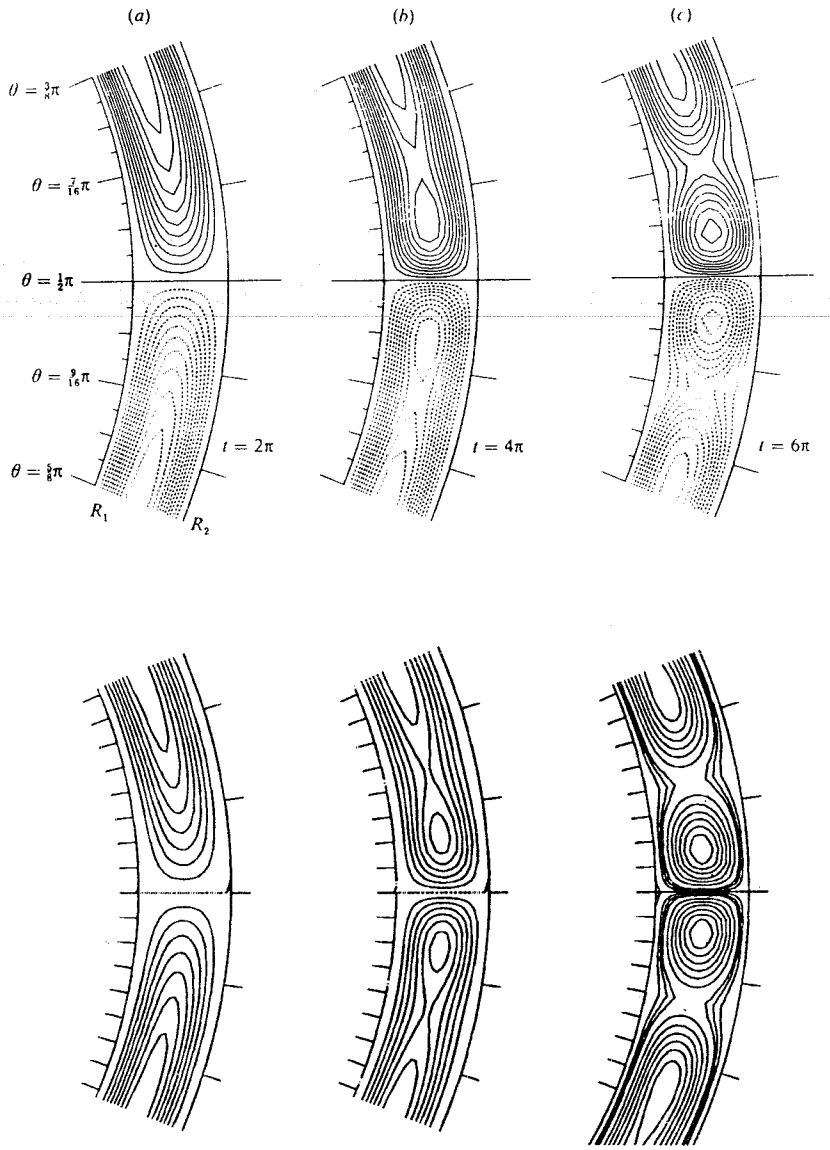

Figure 4(a)–(c). Meridional flow during 0 → 2 transition at $Re = 800$ and $\sigma = 0{\cdot}18$. The tick marks on the outer radius have circumferential spacings equal to the gap width and on the inner radius have angular spacings $\Delta\theta = \pi/64$. Top: results from pseudospectral method.[10] Bottom: present computation

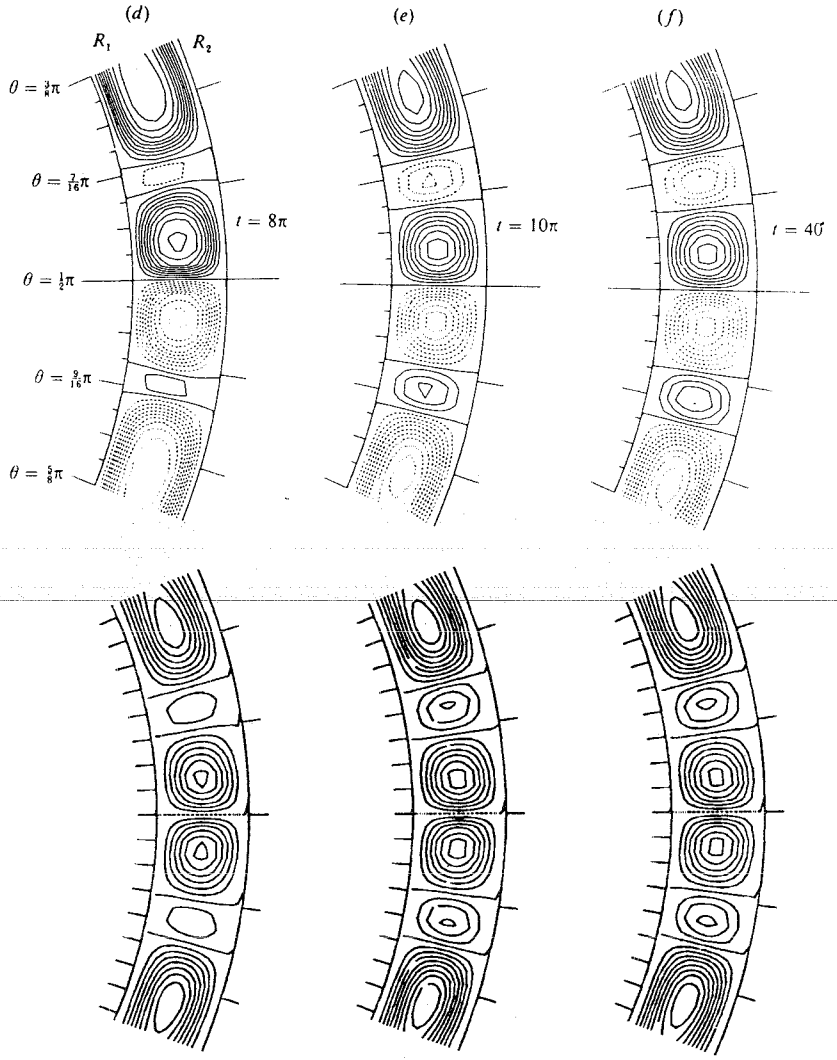

Figure 4(d)–(f) Meridional flow during $0 \rightarrow 2$ transition at $Re = 800$ and $\sigma = 0{\cdot}18$. The tick marks on the outer radius have circumferential spacings equal to the gap width and on the inner radius have angular spacings $\Delta\theta = \pi/64$. Top: results from pseudospectral method.[10] Bottom: present computation

instability. Figure 4 shows a comparison of the meridional flow. The contours are of constant streamfunction $\psi r \sin\theta$, where ψ is related to the meridional velocity component by

$$u_r = \frac{1}{r \sin\theta} \frac{\partial}{\partial\theta}(\psi \sin\theta), \tag{17a}$$

$$u_\theta = -\frac{1}{r} \frac{\partial}{\partial r}(r\psi). \tag{17b}$$

We see that the time-evolving process computed by our method corresponds approximately to that of Reference 10. This demonstrates that the temporal accuracy of the present explicit scheme may be similar to that of pseudospectral methods. However, further modifications to achieve higher-order spatial and temporal accuracy have to be made before the present method can be applied to the simulation of high-*Re* flow.

5. CONCLUSIONS

The purpose of this paper has been to present a study of a numerical method for the solution of the unsteady N–S equations. The proposed method for solving the $\boldsymbol{\omega}$–$\mathbf{u}$ formulation is at least first-order temporally accurate and second-order spatially accurate and is efficient in the computation of moderate-*Re* flow owing to the adoption of an explicit two-stage Runge–Kutta method to advance the vorticity transport equations. Some important aspects of staggered location of the variables, divergence-free correction to the velocity field by a scalar potential and proper approximation of the vorticity boundary condition are examined. In the example of spherical Couette flow, results have demonstrated that the staggered location of velocity and vorticity components satisfies better the solenoidality of the velocity and vorticity fields and that the temporal accuracy of the present method is comparable with that of pseudospectral methods.

ACKNOWLEDGEMENTS

This work was supported by the National Natural Science Foundation and Post-doctoral Science Foundation of China.

REFERENCES

1. F. H. Harlow and J. E. Welch, 'Numerical calculation of time-dependent viscous incompressible flow of fluid with free surface', *Phys. Fluids*, **8**, 2182–2189 (1965).
2. S. C. R. Dennis, D. B. Ingham and R. W. Cook, 'Finite difference methods for calculating steady incompressible flows in three-dimensions', *J. Comput. Phys.*, **33**, 325 (1979).
3. G. Guj and F. Stella, 'Numerical solutions of high-*Re* recirculating flows in vorticity–velocity form', *Int. j. numer. methods fluids*, **8**, 405 (1988).
4. C. G. Speziale, 'On the advantage of the vorticity–velocity formulation of the equations of fluid dynamics', *J. Comput. Phys.*, **73**, 476 (1987).
5. H. F. Fasel, 'Approximation methods for Navier–Stokes problems', in *Lecture Notes in Mathematics*, Vol. 771, Springer, Berlin, 1980, p. 209.
6. P. Orlandi, 'Vorticity–velocity formulation for high *Re* flows', *Comput. Fluids*, **15**, 137 (1987).
7. G. B. Gatski, C. E. Grosch and M. E. Rose, 'The numerical solution of the Navier–Stokes equations for 3-dimensional, unsteady, incompressible flows by compact scheme', *J. Comput. Phys.*, **82**, 298–329 (1989).
8. Y. W. Ma and S. I. Cheng, 'Numerical simulation of turbulent spots', *Acta Aerodyn. Sinica*, No. 4, pp. 35–40 (1984) (in Chinese).
9. G. Guj and F. Stella, 'A vorticity–velocity method for the numerical solution of 3D incompressible flows', *J. Comput. Phys.*, **106**, 286–298 (1993).
10. P. Marcus and L. S. Tuckerman, 'Simulation of flow between concentric rotating spheres, Parts 1 and 2', *J. Fluid Mech.*, **185**, 1–65 (1987).
11. M. Wimmer, 'Experiments on a viscous fluid flow between concentric rotating spheres', *J. Fluid Mech.*, **78**, 317–315 (1976).
12. P. J. Roache, *Computational Fluid Dynamics*, Hermosa, Albuquerque, NM, 1982.